Int. J. Electrochem. Sci., 15 **(2020)** 2752 – 2765, doi: 10.20964/2020.03.02

International Journal of
ELECTROCHEMICAL
SCIENCE
www.electrochemsci.org

Effect of Current Density on Properties of Sol-Enhanced Ni–P–Al_2O_3 Composite Coating

Yongfeng Li[*], *Kun Zhang, Mingming Zhang, Yaqi Zhang, Tingting Wu and Hongyuan Zhao*

School of Mechanical and Electrical Engineering, Henan Institute of Science and Technology, Xinxiang, 453003, China
[*]E–mail: yongfengli121@outlook.com

Received: 26 September 2019 / *Accepted:* 13 November 2019 / *Published:* 10 February 2020

A Ni–P–(sol)Al_2O_3 coating was prepared on the surface of Q235 steel by direct-current electrodeposition. The coating surface morphology and structure were characterized by scanning electron microscopy and energy dispersive spectroscopy, respectively. The wear resistance of the coating was measured by a friction and wear machine. The coating hardness was measured by a microindentation instrument. The coating hardness was measured by a micrometer indentation meter. The corrosion resistance of the coating was tested by an electrochemical workstation. When the current density was 7 A/dm^2, the deposition rate of the Ni–P–(sol)Al_2O_3 composite coating was 83.9 um/h, the surface morphology of the coating was smoothest and finest, and most alumina entered the coating and was distributed more evenly. With an increase in current density, the microhardness of the Ni–P–(sol)Al_2O_3 composite coating first increased and then decreased, and the maximum microhardness was 669.2HV. When the current density was 7 A/dm^2, the coating had the best corrosion resistance and wear resistance.

Keywords: current density, electrodeposition, sol reinforced composite coating, corrosion resistance, wear resistance

1. INTRODUCTION

A large proportion of steel structure in buildings in a country or region may reflect the higher level of local economic development[1] . Few kinds of steel meet steel structural requirements, and Q235 steel is used most widely [2] . Corrosion of iron and steel can easily lead to structural failure and safety accidents, which causes huge economic losses, and leads to environmental pollution. Therefore, iron and steel anti–corrosion is of great significance[3] . Surface electrodeposition[4] is an effective method to improve the corrosion resistance of iron and steel. Common coatings include Ni, Zn and Cr [5-7] . The electrodeposition process is flexible, and the electrodeposited coating has the advantages of

a high density and a low porosity. Electrodeposition is an effective means to improve the wear resistance and corrosion resistance of the coating.

With rapid developments in modern industry, it is difficult for traditional single-metal coating properties to meet special requirements of some harsh environments, and more people have given increased attention to multifunctional alloy coatings with special surface properties[8-10] . Composite coatings have a higher hardness and a better corrosion resistance than single metal coatings. Electroplating Ni – Zn alloy is a high corrosion–resistance alloy coating that has been developed based on galvanizing in recent years. Its corrosion resistance is 4–8 times that of a pure zinc coating. When the mass fraction of nickel in the coating varies between 8% and 15%, the corrosion resistance of the alloy with 13% nickel is best[11] . The deposition rate of Ni–P alloy is rapid. The stability and cost of the plating solution are good, and its amorphous structure is good. The coating corrosion resistance and wear resistance are excellent. The Vickers hardness reaches ~1000HV when it is heat treated at an appropriate temperature. Under these conditions, the coating wear resistance is comparable to that of hard chromium coating[12-14] .

With the development of electrodeposition technology and nano-technology, research into nanocomposite coatings has become the focus of attention of scholars globally[15] . Second – phase particles, such as nanoscale SiO_2[16,17], Al_2O_3[18-20], TiO_2[21], SiC[22], PTFE[23, 24], ZrO_2[25], and graphene[26],were introduced to strengthen the coating. However, the composite coatings may be problematic. Because nanoparticles have a high-energy surface and activity, these nanoparticles are unstable and agglomerate easily in the plating bath without special surface modification. The dispersant selection and requirements are more onerous, and it is not easy to grow dispersants uniformly on the matrix surface. Therefore, the homogeneous quality is affected and the coating mechanical properties are weakened. A sol can avoid nanoparticle agglomeration in the coating matrix[27–29] , and it is dispersed rapidly and uniformly in the plating solution, which allows for easy dopeding, and the required external conditions are easy to achieve.

A Ni–P–(sol)Al_2O_3 coating was prepared on the surface of Q235 steel by electrodeposition. An Al_2O_3 sol was used instead of nanopowder. The effects of current density on the morphology, hardness, corrosion resistance and friction and wear of the coatings were studied.

2. EXPERIMENT AND METHODS

2.1 Sample Preparation

The substrate specimen used in the experiment was a 40 mm × 25 mm × 2 mm Q235 cold-rolled steel sheet. Prior to the deposition experiments, the substrate was polished with 400, 800 and 1000 grade SiC paper, and then washed and rinsed with distilled water.

Workpieces were inevitably contaminated with oil during processing, storage and transportation. The oil removal formula that was used in the experiment is shown in Table 1. The workpieces were cleaned with deionized water and ultrasonic cleaning was carried out for 2min.

Table 1. Components of alkali cleaning solution and technological conditions

Composition	Quantity(g/L)	Drugs and parameters	Quantity
NaOH	35	OP-10	2 (g/L)
Na_2CO_3	25	Temperature	85± 2(℃)
Na_3PO_4	10	Time	10–20(min)
Na_2SiO_3	10		

Pickling was used to remove oxide film, oxide scale and rust on the metal surface after oil removal. Hydrochloric acid has a strong solubility for metal oxides, a slow dissolution to iron and steel matrix, and a clean surface after pickling, but it produces extensive acid mist, which corrodes equipment. Sulfuric acid is less corrosive to the matrix and produces less acid mist, but it is prone to over–corrosion and hydrogen embrittlement. In this experiment, a mixture of 15 wt% nitric acid and 5 wt% phosphoric acid was used as a pickling solution. and 5 wt% hydrochloric acid was used for activation. The activation time was 3 min at room temperature (~25°C) After activation, ultrasonic cleaning was used for 1 min prior to plating. To obtain a clean surface, and after each step, all samples were washed with distilled water.

2.2 Bath composition and process conditions

The formula of the Ni–P plating basic plating solution that was used in the test was: $NiSO_4 \cdot 6H_2O$ 120g/L,H_3BO_3 30 g/L,$NaH_2PO_2 \cdot H_2O$ 15 g/L,$NiCl_2 \cdot 6H_2O$ 20 g/L,$C_6H_8O_7$ 40 g/L,$C_{12}H_{25}SO_4Na$ 0.4 g/L and pH 3.5, and the temperature was 55°C. Al_2O_3 sol was used instead of nanopowder. The alumina sol specifications were: the alumina sol concentration was 20% and the average particle size was 60–70 nm. Sol (80 mL/L) was added to the Ni–P base plating bath. The plating solution was stirred mechanically with a magnetic stirrer. The main components of the composite plating solution were:

Table 2. Compositions of bath solution

Bath compositions	Concentration ($g \cdot L^{-1}$)	Depositing parameters	Values
$NiSO_4 \cdot 6H_2O$	120	Temperature (℃)	55
H_3BO_3	30	pH	3.5
$NaH_2PO_2 \cdot H2O$	15	Current density (A/dm^2)	4,5,6,7,8,9
$NiCl_2 \cdot 6H_2O$	20	Time (min)	10
Al_2O_3 sol wt20% (60–70nm)	80(mL/L)		
$C_{12}H_{25}SO_4Na$	0.4		

After pretreatment, the samples were placed rapidly into the plating bath for 10min. After electroplating, the specimen was removed from the plating bath and washed with distilled water and dried for performance testing.

2.3 Performance of sol composite plating layer

2.3.1 Micromorphology and structural analysis of the plating layer

The surface morphology of the coating was observed by Quanta 200 scanning electron microscopy (SEM) and the elemental composition of the plating layer was measured by energy dispersive X–ray spectroscopy (EDS).

2.3.2 Determination of plating rate

The coating plating speed is usually measured by the thickness or weighing method. In this experiment, the weighing method was used. The weighing method involves an AL204 electronic analytical balance produced by Maitler Instrument Co., Ltd. The samples were washed and dried with distilled water after pickling. The masses before and after plating were measured. The pattern length, width and height were measured using a digital vernier caliper, and the surface area of the pattern was calculated by size. The formula for determining the plating rate was:

$$V = (G_2 - G_1)/(S \cdot \rho \cdot t) \times 10^4 \quad (1)$$

where:

V is the deposition rate of the plating layer (μm/h);

G_1 is the mass before the test block was plated (g);

G_2 is the mass of the test block after plating (g);

ρ is the density of alloy plating layer (g/cm^3);

S is the plating surface area of the test block (cm^2) and

t is the plating time (h)

2.3.3 Abrasion resistance test

The Vickers microhardness measurements of the coatings were taken using a VMH–002V microhardness tester at a load of 50 g for 15 s. The corresponding final values were reported as the average of five measurements. The friction and wear properties of the coatings were tested using a MS–T3000 ball–disc friction and wear tester. Quenched 3-mm-diameter steel balls were selected as grinding materials. The temperature was 25–30°C, and the relative humidity was 25%±10%. The applied load was 500g, the motor speed was 300r/min, and the duration was 15min.

2.3.4 Corrosion resistance

The polarization curve of the anode was measured at room temperature using a CS2350 electrochemical workstation, and the corrosion resistance of the coating was evaluated by a Tafel curve. The coating was exposed to a scanning range of –2.0– 1.0 V at a scanning rate of 1 mV/s in 3.5 wt% NaCl solution. The auxiliary electrode was a platinum electrode and the reference electrode was a saturated calomel electrode.

3. RESULTS AND DISCUSSION

3.1 Effect of current density on deposition velocity

The specific experimental parameters were: temperature 55 °C, pH 3.5; and current density 4 A/dm^2, 5 A/dm^2, 6 A/dm^2, 7 A/dm^2, 8 A/dm^2, 9 A/dm^2, respectively. The plating time was 10 min. Figure 1 shows the electrodeposition rates that were measured at six different current densities. With the increase in current density, the deposition rate of the Ni – P – (sol)Al_2O_3 composite coating first increased and then decreased. When the current density was 7 A/dm^2, the deposition rate reached a maximum of 83.9um/h. When the current density exceeded 7 A/dm^2, the deposition rate of the Ni–P–(sol)Al_2O_3 composite coating decreased because the Ni^{2+} resistance in the plating bath system was constant during plating, and the electrodeposition rate depends mainly on the reduction rate of Ni^{2+} on the cathode. The increasing current density accelerated of electron movement, which led to an increase in electron yield rate of Ni^{2+} and the natural increase of a reduced Ni^{2+} so that the deposition rate was accelerated.

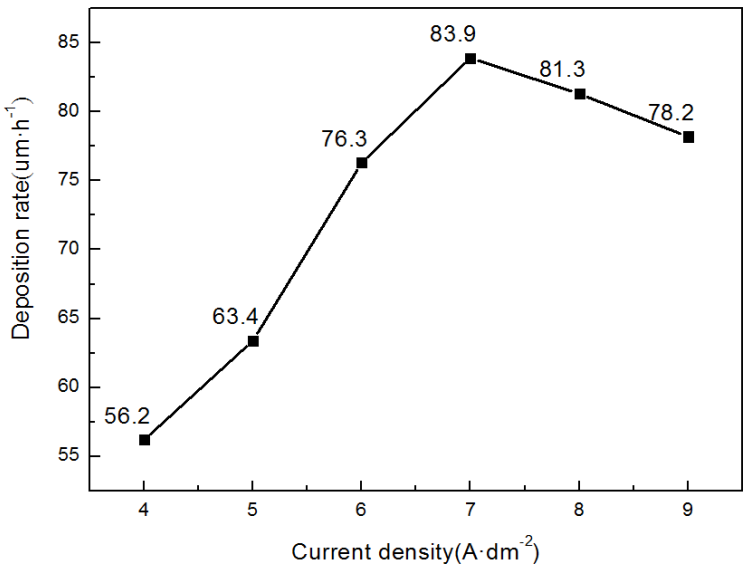

Figure 1. Effect of current density on deposition rate. Coatings prepared under different current densities of 4 A/dm^2, 5 A/dm^2, 6 A/dm^2, 7 A/dm^2, 8 A/dm^2 and 9 A/dm^2 respectively. Temperature 55 °C, pH 3.5, plating time 10 min.

With an increase in cathodic polarization potential, the electric field force near the plated sample increased. As the pulling force of the matrix increased, the migration rate of Ni^{2+} to the matrix accelerated, and the concentration of Ni^{2+} near the matrix was relatively high, which increased the reduction and deposition rates significantly. When the current density exceeded 7 A/dm^2, the coating grew too fast on the substrate. The deposition rate continued to increase, but the experimental phenomenon shows that the coating was "slagging" and washed away by the bath. After plating powder particles precipitated on the surface at a high current density, and the coating mass decreased after washing, which led to a decrease of calculated deposition rate. Therefore, when the current density was 7 A/dm^2, the microhardness value of the sol composite coating was best.

3.2 Coating Hardness

Figure 2 shows the relationship between the current density and the coating microhardness. The specific experimental parameters were temperature 55 °C, pH 3.5 and current density 4 A/dm^2, 5 A/dm^2, 6 A/dm^2, 7 A/dm^2, 8 A/dm^2, 9 A/dm^2, respectively. The plating time was 10 min. Figure 2 shows that the microhardness of the Ni–P–(sol)Al_2O_3 composite coating increased with an increase in current density. When the current density was 7A/dm^2, the microhardness of the Ni–P–(sol)Al_2O_3 composite coating reached a maximum of 669.2HV. The high hardness of the alumina particles themselves may be the main reason for the microhardness of the Ni–P–(sol)Al_2O_3 composite coating being higher than that of the Ni–P coating[30]. The microhardness of the Ni–P–(sol)Al_2O_3 composite coating showed a downward trend when the current density exceeded 7A/dm^2 because nickel ions were deposited on the matrix with the particles with the increase in current density. Furthermore, the contact area between the particles and the coating increased, which increased the number of particles that reached the matrix. Particles were embedded in the coating by weak and strong adsorption[31], which makes the coating dispersive and fine–grained strengthening, and makes the coating more compact and harder. The nanoparticles improve the matrix grain refinement, which improves the nanocomposite coating microhardness. Therefore, as the nanoparticle content in the coating increased, the composite coating microhardness increased gradually, and the mechanical properties of the coating improved[32]. However, when the current density exceeded 7 A/dm^2, the movement of nickel ions is was controlled mainly by current migration. A higher current density increased the alumina–particle encapsulation by the nickel ions. The faster the growth of the coating on the substrate surface per unit time, the more easily the alumina particles in the coating agglomerate[33]. Therefore, the internal coating structure was loose, the distribution of alumina particles was uneven, and the hardness decreased.

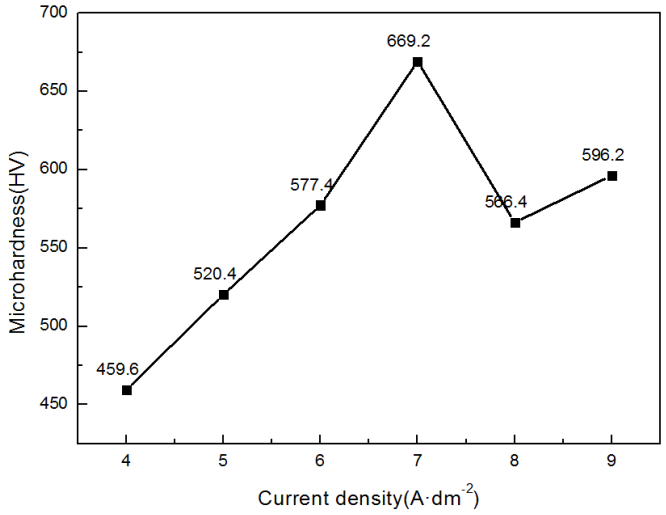

Figure 2. Effect of current density on coating hardness. Coatings prepared under different current densities of 4 A/dm^2, 5 A/dm^2, 6 A/dm^2, 7 A/dm^2, 8 A/dm^2 and 9 A/dm^2 respectively. Temperature 55 °C, pH 3.5, plating time 10 min.

3.3 coating structure and surface morphology

Figure 3 shows the surface morphologies of the composite coating that were obtained for different current densities. Figure 4 shows the EDS spectrum of the Ni–P–(sol)Al_2O_3 composite coating. Table 3 shows that the atomic percentage of Al increases with an increase in current density. Figure 3 shows that when the current density is 4–7/dm^2, as shown in Figure 3(a) to Figure 3(d), the surface morphology of the coating changes visibly with an increase in current density. Particles on the coating surface change gradually from an irregular spherical to a regular spherical shape, and the particles become smaller. The incorporation of nanoalumina changes the crystal growth orientation and morphology of the substrate surface significantly. The use of nanoalumina particles as the center of nuclear formation has an inhibitory effect on Ni crystal growth [34]. The particle distribution changes gradually from a scattered distribution to a uniform distribution, and the degree of particle dispersion decreases from large to small, which makes the coating more compact. When the current density is 7A/dm^2, the coating is densest, and the alumina enters the coating most and distributes most evenly. When the current density exceeds 7A/dm^2, the particle shape on the surface of the coating changes from a regular sphere to an irregular slender strip, and many particles accumulate, which results in agglomeration. This behavior arises because the current density plays an important role in particle the growth and adsorption on the surface of the substrate during electrodeposition. The migration rate of Ni^{2+} to the matrix is accelerated with an increase in current density; the alumina particles that are removed from the plating bath increase in unit time, and the crystals that grow on the matrix surface gradually convert to regular spheres. However, the coating deposition rate increases too rapidly when the current density exceeds a certain limit. The particles on the substrate have not yet been arranged closely. They are adsorbed by the excessive current and cover the growth, which results in a loosening of their internal structure. The larger current density provides energy for particle agglomeration on the

coating surface, which worsens the coating surface roughness and densification. The pattern edge appears burned and a blackening phenomenon results when the current density is 9A/dm^2.

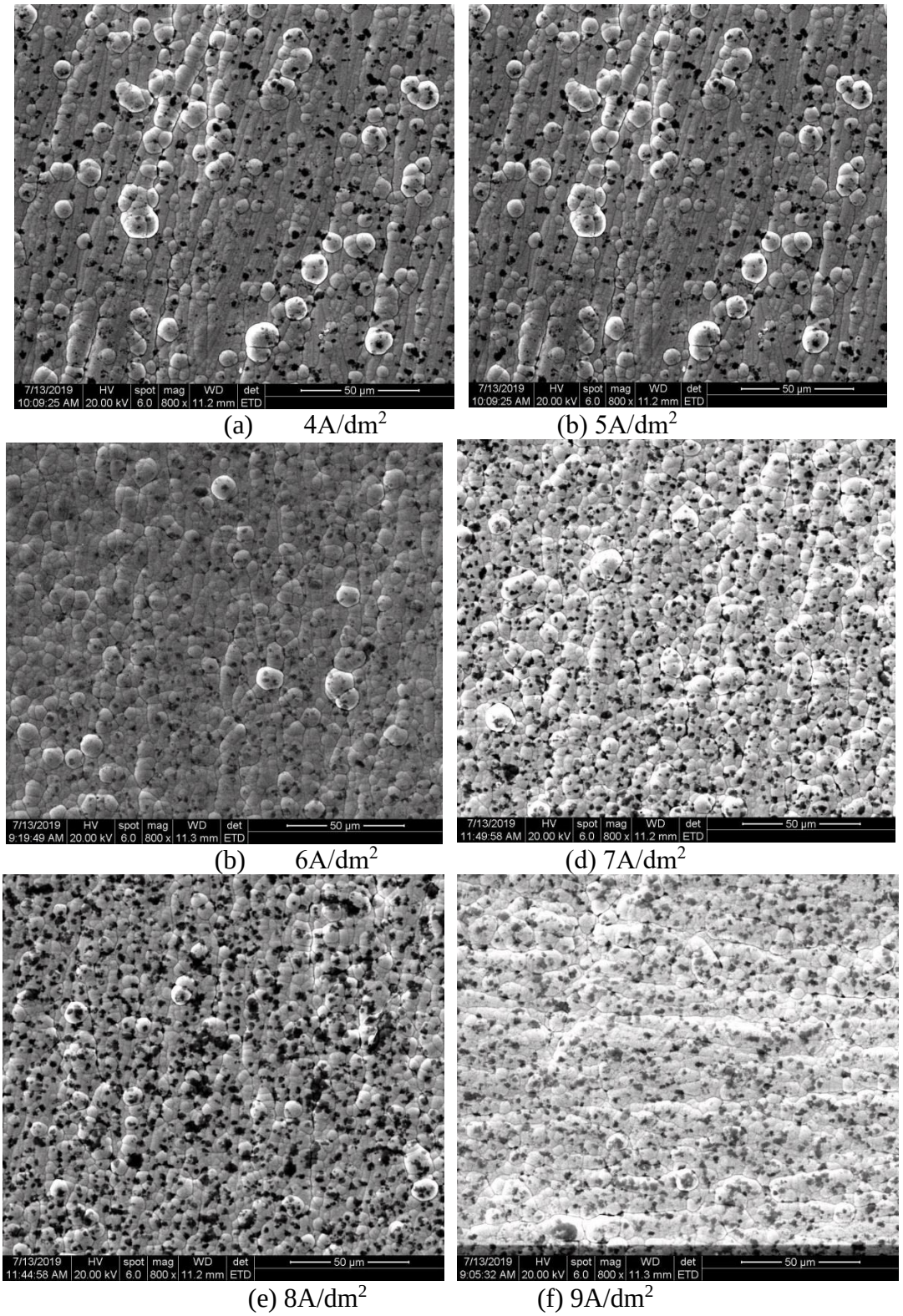

Figure 3. Surface morphology of coatings prepared under different current densities. Current density (a)4 A/dm^2, (b)5 A/dm^2, (c)6 A/dm^2, (d)7 A/dm^2, (e)8 A/dm^2, (f)9 A/dm^2, temperature 55 °C, pH 3.5, plating time 10 min.

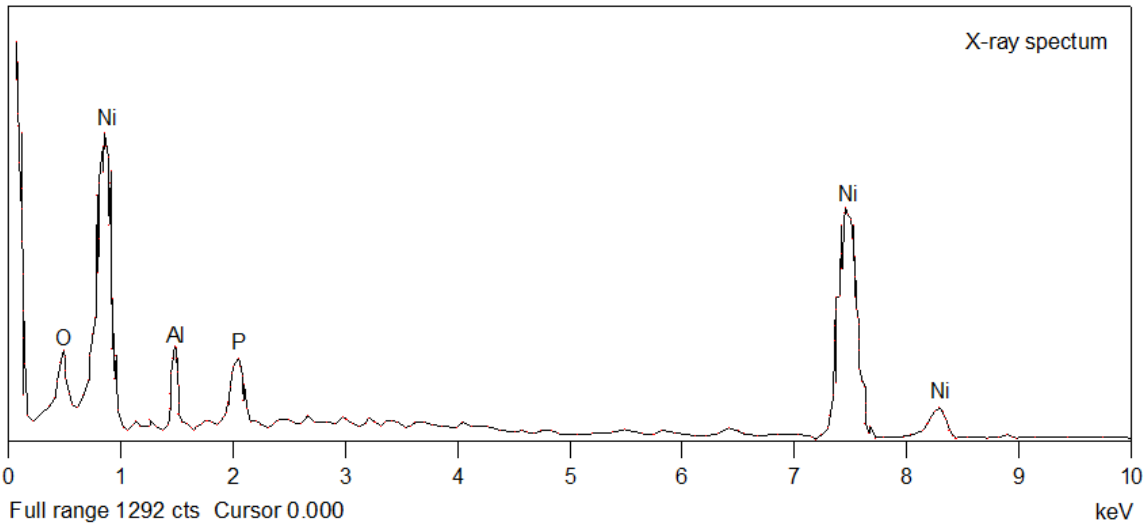

Figure 4. EDS spectrum of Ni–P–(sol)Al_2O_3 composite coating prepared under current densities of 7 A/dm^2. Temperature 55 °C, pH 3.5, plating time 10 min.

Table 3. Aluminum content of coatings prepared under different current densities

Current density (A/dm^2)	4	5	6	7	8	9
Atomic percentage of Al element	1.30	2.23	2.76	3.01	3.21	3.44

3.4 Corrosion resistance of coating

Figure 5 shows the corrosion polarization curves of the Ni–P–(sol) Al_2O_3 composite coatings that were obtained at different current densities in 3.5% NaCl solution. The co-deposited particles in the nickel matrix can reduce the passivation and corrosion resistance of the nanocomposite coating. Therefore, the corrosion resistance of the Ni–P coating decreases with the addition of alumina particles[35]. Figure 5 shows that with an increase of current density, the self–corrosion potential of the coating moves to a negative direction. The composite coating has the most positive self–corrosion potential –0.394V when the current density is 4A/dm^2 and the self–corrosion potential of the coating moves to –0.438V when the current density increases to 7 A/dm^2. Therefore, the corrosion resistance of the coating increases with an increase in current density.

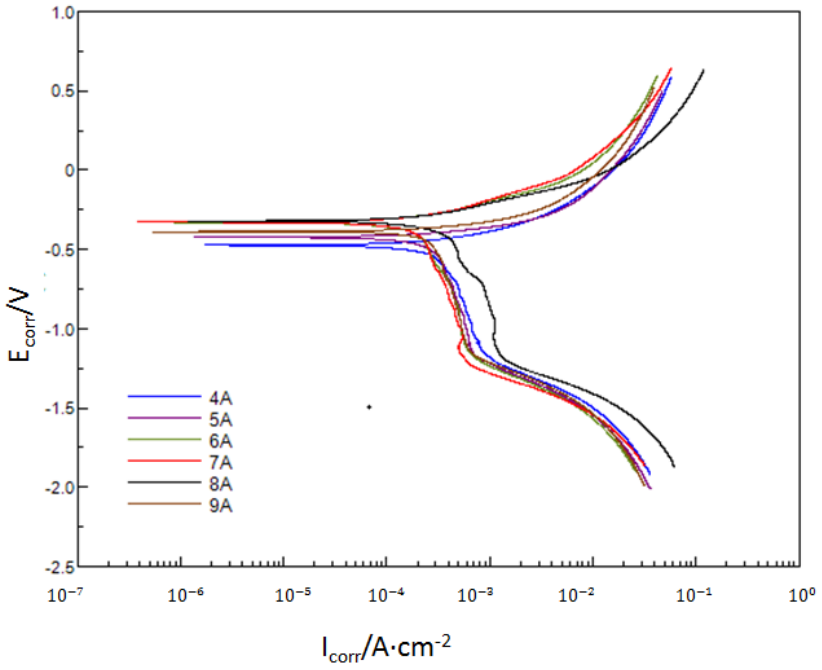

Figure 5. Polarization curves of coatings prepared under different current densities of 4 A/dm^2, 5 A/dm^2, 6 A/dm^2, 7 A/dm^2, 8 A/dm^2 and 9 A/dm^2 respectively. Temperature 55 °C, pH 3.5, plating time 10 min.

The data in Table 4 were fitted automatically by a Tafel curve in Figure 4. Table 4 shows that with an increase in current density, and when the current density ranges of 4 to 7A/dm^2, corrosion potential, corrosion current density and corrosion rate decreased. When the current density was 4A/dm^2, the maximum corrosion current density was 8.09×10^{-4}A/cm^2 and the maximum corrosion rate was 9.369mm/a. The corrosion potential decreased with an increase in current density. When the current density exceeded 7A/dm^2, the corrosion current density and corrosion rate tended to increase. When the current density is 7A/dm^2, the corrosion potential is –0.438V, the minimum corrosion current density was 4.18×10^{-4}A/cm^2 and the minimum corrosion rate was 4.845mm/a.

Table 4. Important polarization curve parameters

Current density /A • dm^{-2}	Corrosion potential /V	Corrosion current density /A • cm–2	Corrosion rate /mm•a − 1
4	− 0.394	8.09×10^{-4}	9.369
5	− 0.326	6.66×10^{-4}	7.708
6	− 0.479	5.79×10^{-4}	6.710
7	− 0.438	4.18×10^{-4}	4.845
8	− 0.334	4.35×10^{-4}	5.036
9	− 0.392	4.86×10^{-4}	5.627

With the increase in current density, the deposition rate of the matrix metal Ni increased. The grain size decreased, which made the coating more compact and improved the coating corrosion resistance. However, excessive current density led to serious hydrogen evolution on the cathode surface, which resulted in the blockage of alumina particles that entered the coating and the dispersion of alumina particles in the coating. The compactness and corrosion resistance of the coating decreased. Therefore, the corrosion resistance of the Ni–P–(sol) Al_2O_3 composite coating was best when the current density was 7A/dm^2,

3.5 Coating wear resistance

Figure 6 shows the variation curve of the friction coefficient of the Ni–P–(sol)Al_2O_3 composite coating with time for different current densities. The high friction coefficient of the nanocomposite coating may be related to the incongruity of the hard alumina particles in the coating. However, the wear resistance of the composite coating can be improved by nano‐alumina. The increase in alumina particle numbers in the coating can improve the wear resistance of the nanocomposite coating[36]. This behavior was confirmed by Figure 3 (d) and Table 3. Figure 6 shows that the friction coefficient of each sample increases rapidly at the beginning of the friction coefficient measurement. This increase results mainly from the fact that the macro–stress field that is caused by the microprotuberant particles on the sample surface becomes a dispersed stress field without matrix polishing. The microprotrusions on the friction contact surface become plastic deformation with the friction process proceeded, the surface of the sample becomes smooth gradually and the friction coefficient tends to be stable. Table 5 shows that the average friction coefficient of the Ni–P–(sol)Al_2O_3 composite coating is smallest when the current density is 4A/dm^2. When the current density was 9A/dm^2, the average friction coefficient of the composite coating was largest. Figure 7 shows that with an increase in current density, the wear rate of the coating first decreased and then increased. When the current density was 7A/dm^2, the wear rate of the Ni–P–(sol)Al_2O_3 composite coating was the lowest, at 1.768×10^{-6}g • m^{-1} because the alumina particles enter the coating less and the "microprotuberance" phenomenon in the coating is not obvious when plating occurs at a low current density. Therefore, the friction coefficient is lower, but the wear rate is higher in the friction and wear experiment. Al_2O_3 particles have a high hardness and wear resistance, and support the friction surface load during the friction process, reduce the matrix alloys wear and resist plastic deformation. When the current density is high, the grain growth is uneven, the structure is loose and the wear resistance is weak. Therefore, when the current density is 7A/dm^2, the wear rate of the composite coating is lowest and the wear resistance is best.

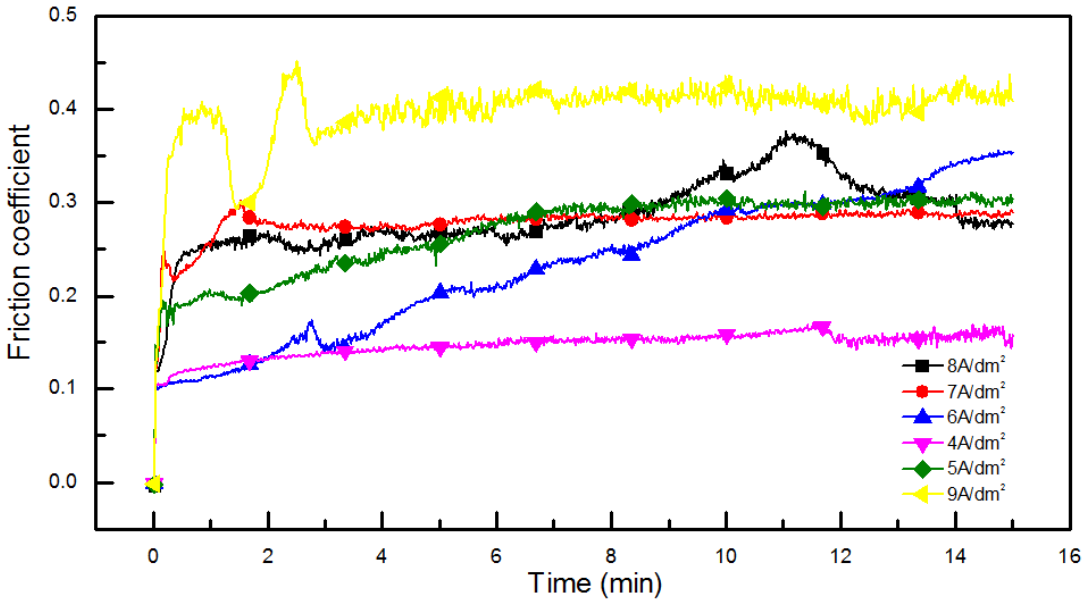

Figure 6. Friction coefficient versus time curve of coatings prepared under different current densities of 4 A/dm^2, 5 A/dm^2, 6 A/dm^2, 7 A/dm^2, 8 A/dm^2 and 9 A/dm^2 respectively. Temperature 55 °C, pH 3.5, plating time 10 min.

Table 5. Friction factors of coatings prepared under different current densities

Current density (A/dm^2)	4	5	6	7	8	9
Average friction coefficient	0.1427	0.2690	0.2332	0.2784	0.2851	0.3975

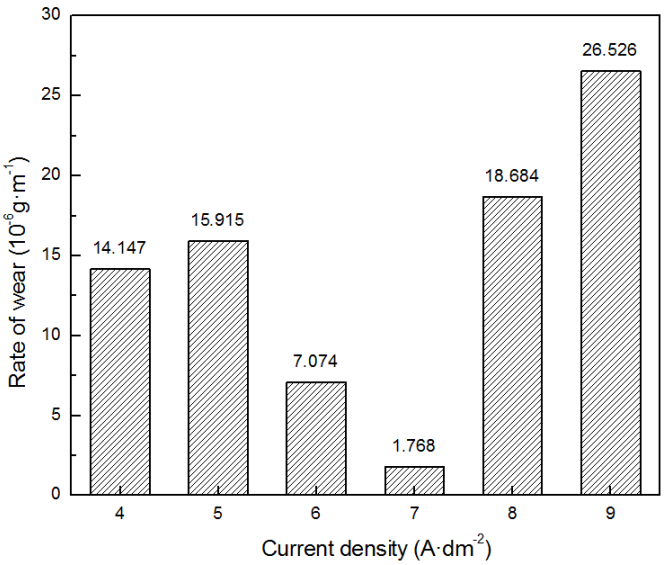

Figure 7. Wear rate of coatings prepared under different current densities of 4 A/dm^2, 5 A/dm^2, 6 A/dm^2, 7 A/dm^2, 8 A/dm^2 and 9 A/dm^2 respectively. Temperature 55 °C, pH 3.5, plating time 10 min.

4. CONCLUSIONS

1. As the current density increases from 4A/dm^2 to 9A/dm^2, the plating rate increased first and then decreased. When the current density is 7A/dm^2, the fastest plating speed was 83.9um/h.

2. From the surface morphology of the coating, the distribution of nano–alumina in the coating was more uniform and the content of nano–alumina increased with an increase in current density. When the current density was 7A/dm^2, the coating was most dense, and the alumina entered the coating most and distributed most evenly.

3. According to the electrochemical corrosion resistance test, the best corrosion resistance among the six current densities was 7A/dm^2, the corrosion potential was –0.438V, the corrosion current density was 4.18×10^{-4}A/cm^2, and the corrosion rate was 4.845mm/a. The worst corrosion resistance was 4A/dm^2.

4. The Ni–P–(sol) Al_2O_3 composite coating had good friction and wear properties. With the increase in current density, the microhardness of the composite coating increased first and then decreased, and the friction coefficient increased, but the wear rate decreases gradually. When the current density was 7A/dm^2, the composite coating microhardness reached 669.2HV. At the same time, the friction and wear properties were best, and the wear rate was 1.768×10^{-6}g·m^{-1}.

ACKNOWLEDGMENTS
The authors gratefully acknowledge the supports from the Key Scientific Research Projects of Higher Education of Henan Province of China (19A430014), the Young Key Teachers Projects in Henan Higher Education Institutions (2018GGJS113), Scientific and Technological Research Projects of Henan Province(192102210215) and Program for Innovative Research Team (in Science and Technology) in University of Henan Province (20IRTSTHN016). We thank Laura Kuhar, PhD, from Liwen Bianji, Edanz Group China (www.liwenbianji.cn/ac), for editing the English text of a draft of this manuscript.

References

1. F Wald, L. Simo˜es, D Moore, T. Lennon, M. Chladna, A. Santiago, M. Benes, L. Borges, *J. Fire Saf.*, 41 (2006) 509.
2. Y.Z. Xu, Z. Sun and Y.Q. Zhang,Adv. *Mater. Sci. Eng.*, 2016 (2016) 10.
3. P. Qiu, F. Li, X. L. Sun, P. P. Gao, L. G. Yang, C. F. Chen and L. Ge, *Chemistryselect*,24 (2019) 7151.
4. C. S. Liu, F. H Su and J. Z. Liang, *Trans. Nonferrous Met. Soc. China*, 28 (2018) 2489.
5. W. Lan, S. Zhao and W. Zhou, *Materials Express*, 8(2018) 245.
6. C. Somphotch, H. Hayashibara, A. Ooi, E. Tada and A. Nishikata, *J. Electrochem. Soc.*, 165 (2018) 590.
7. D. Q. Zhao, X. Jiang, Y. X. Wang, W. S. Duan and L. P. Wang, *Appl. Surf. Sci.*, 457 (2018) 914.
8. A. Laszczynska, W. Tylus, B. Szczygiel, and I. Szczygieł, *Appl. Surf. Sci.*, 462 (2018) 432.
9. H. Liu, G. C. Chen, L. Z. Du, H Lan,C. B. Huang,B. L. Wang, H. Y. Zhang and W. G. Zhang, *Rare Met. Mater. Eng.*, 47 (2018) 647.
10. Y. F. Li, C. G. Fu, L. L. Liu, M. C. Liang, Y. M. Liu and W. Gao, *Int. J. Mod. Phys. B.*, 33 (2019) 1.
11. J. Xu, T. D. Hall, M. E. Inman, E. J. Taylor and S. Snyder, *The 231st Ecs Meeting*,77 (2017) 1237.
12. A. Hadipour, M. Rahsepar and H. Hayatdavoudi, *Surf. Eng.*, 35 (2019) 883.

13. J. D. Lin and C. T. Chou, *Surf. Coat. Tech.*, 368 (2019) 126.
14. A. Bahramian, M. Eyraud, F. Vacandio and P. Knauth, *Surf. Coat. Tech.*, 345 (2018) 40.
15. S. Ahmadiyeh, A. Rasooli and M. G. Hosseini. *Surf. Eng.*, 35 (2019) 861.
16. S. Sadreddini, S. R. Ardakani, H. Rassaee. *J. Mater. Eng. Perform.*, 26 (2017) 2032.
17. S. Sadreddini, Z. Salehi, and H. Rassaie, , *Appl. Surf. Sci.*, 324 (2015) 393.
18. Y. Zhang, M. Kang, H. Z. Li and Y. T. Liu, *Int. J. Electrochem. Sci.*, 14 (2019) 6032.
19. R. Hu, Y. Y. Su, Y. R. Liu, H. D. Liu,Y. M. Chen, C. S. Cao and H. T. Ni, *Nanoscale Res. Lett.*, 1(2018) 1.
20. P. Gadhari and P. Sahoo, *Silicon*, 129 (2017) 844.
21. Y. F. Li, L. M. Zhao, Z. K. Wang, L. J. Ma, J. X. Su,C. Chang and M. C. Jiao, *Int. J. Electrochem. Sci.*, 12 (2017) 3385.
22. A. Farzaneh, M. Ehteshamzadeh, M. Can, O. Mermer and S. Okur, *Prot. Met. Phys. Chem*, 52 (2016) 632.
23. C. H. Lin, J. R. Lee, P. G. Teng, S. Y. Tsai, H. H. Sheu, K. H. Hou, and M. D. Ger, *Int. J. Electrochem. Sci.*, 13 (2018) 3147.
24. M. Tajbakhsh, O. Yaghobizadeh, M. F. Nia, *P I MECH ENG C–J MEC*, 233 (2019) 94.
25. F. Tabatabaei, S. Vardak, S. Alirezaei and K. Raeissi, *KOVOVE MATER*, , 56 (2018) 379.
26. C. Liu, D. D. Wei, X. Y. Huang,Y. J. Mai, L. Y. Zhang and X. H. Jie, *J. Mater. Res. Technol.*, 50 (2019): 2331.
27. W. W. Chen, Y. D. He, Wei Gao, *Surf. Coat. Tech.*, 204 (2010) 2487.
28. A. Sadeghzadeh–Attar, G. AyubiKia and M. Ehteshamzadeh, *Surf. Coat. Tech.*, 307 (2016) 837.
29. Y. X. Wang, D. Cao, W. D. Gao,Y. X. Qiao, Y. X. Jin,G. Chen,W. Gao and Z. Zhi, *J. Alloys Compd*, 792 (2019) 617.
30. S. Alirezaei, S. M. Monir Vaghefi, M. Urgen, A. Saatchi, and K. Kazmanli, *J. Compos. Mater.*, 47 (2013) 3323.
31. F. C. Walsh, C. T. J. Low, J. O. Bello. *Transactions of the Imf.*, 93 (2015) 147.
32. R. MafiIman and C. Dehghanian, *Appl. Surf. Sci.*, 258 (2011) 1876.
33. S. Sadreddini,S. Rahemi Ardakani and H. Rassaee, *J. Mater. Eng. Perform.*, 26 (2017) 2032.
34. Q. Y. Feng, T. J. Li, H. Y. Yue,K. Qi,F. D. Bai and J. Z. Jin, *Appl. Surf. Sci.*, 254 (2007) 2262.
35. H. Shahbazi, M. Mahdavi, S. Alirezaei and F. Tabatabaei, *Mater. Res. Express*, 6 (2019) 8.
36. A. Sharma and A.K. *Singh, J. Mater. Eng. Perform.*, 22 (2013) 176.